J Mol Model (2012) 18:3541–3552
DOI 10.1007/s00894-012-1355-x

ORIGINAL PAPER

Modeling the weak hydrogen bonding of pyrrole and dichloromethane through Raman and DFT study

Dheeraj Kumar Singh · Birendra Pratap Asthana · Sunil Kumar Srivastava

Received: 12 August 2011 / Accepted: 4 January 2012 / Published online: 11 February 2012

Abstract Raman spectra of neat pyrrole (C_4H_5N) and its binary mixtures with dichloromethane (CH_2Cl_2, DCM) with varying mole fractions of C_4H_5N from 0.1 to 0.9 were recorded in order to monitor the influence of molecular interaction on spectral features of selected vibrational bands of pyrrole in the region 600-1600 cm^{-1}. Only 1369 cm^{-1} vibrational band of pyrrole shows a significant change in its peak position in going from neat pyrrole to the complexes. The 1369 cm^{-1} band shows (~6 cm^{-1}) blue shift upon dilution and the corresponding linewidth shows the maximum shift at C=0.5 mole fraction of pyrrole upon dilution which clearly indicates that the concentration fluctuation model plays major role. Quantum chemical calculation using density functional theory (DFT) and ab-initio (MP2 and HF) methods were performed employing high level basis set, 6-311++G(d,p) to obtain the ground state geometry of neat pyrrole and its complexes with DCM in gas phase. Basis set superimpose error (BSSE) correction was also introduced by using the counterpoise method. In order to account for the solvent effect on vibrational features and changes in optimized structural parameters of pyrrole, polarizable continuum model (PCM) (bulk solvations) and PCM (specific plus bulk solvations) calculations were performed. Two possible configurations of pyrrole + DCM complex have been predicted by B3LYP and HF methods, whereas the MP2 method gave only single configuration in which H atom of DCM is bonded to π ring of the pyrrole molecule. This affects significantly the ring vibrations of pyrrole molecule, which was also observed in our experimental results.

Keywords Binary mixture ($C_4H_5N + CH_2Cl_2$) · Intermolecular interaction · Quantum chemical calculations · Raman study

D. K. Singh · B. P. Asthana
Department of Physics, Banaras Hindu University,
Varanasi 221005, India

S. K. Srivastava (✉)
Department of Pure and Applied Physics,
Guru Ghasidas University,
Koni,
Bilaspur 495009, India
e-mail: kashisunil77@gmail.com

Introduction

Intermolecular interactions play fundamental role in understanding the mechanism of various chemical, biological and physical processes [1–6]. One of the most important intermolecular interactions, especially in chemical and biological systems, is hydrogen bonding, which can be monitored by studying the solute-solvent interactions in the model systems using different experimental and theoretical methods. Hydrogen bonds are known to play an important role in stabilizing the secondary and tertiary structures of proteins and provide important clues to understand the molecular recognition [7]. The different biomolecules exhibit hydrogen bond formations, which are so crucial for regulating functions in living systems. Spectroscopic studies of weakly bound intermolecular complexes at conditions of supersonic expansion provide a wealth of information on the structures and dynamics of such species [8] and define a starting point for detailed understanding of various macroscopic phenomena.

The Raman and IR spectra, which arise due to vibrational motion of the atoms in a molecule, are important experimental techniques to probe the intermolecular interactions. Raman spectroscopic techniques are ideally suited to monitor hydrogen bonding [9] since one can extract both structural and dynamic information [9, 10]. The wavenumber

position of a vibrational band relates to the inter-atomic force constants, which are dependent on the electronic structure and bonding, whereas the linewidth contains information regarding molecular dynamics. Several binary mixtures with different hydrogen donor solvents, H_2O, CH_3OH and C_2H_5OH have been studied in the last two decades [11–19], where hydrogen bonding interaction results in a variety of changes in the spectral features.

The microwave spectrum of the pyrrole–water complex was studied almost a decade ago by Tubergen et al. [20]. In this study, accurate rotational constants as well as ^{14}N nuclear quadrupole coupling constants were determined. It is to be noted that the latter quantity was found to be a sensitive gauge of hydrogen bonding. Martoprawiro and Bacskay [21] reported an ab-initio quantum chemical study of the hydrogen bonded (HB) binary complexes of pyrrole–water and pyridine–water and concluded that both pyrrole–water and pyridine–water complexes have hydrogen bonds of similar strength, even though in the former, water acts as a proton acceptor, while it acts as a donor in the latter. Theoretical (ab-initio and DFT) study of the structure and torsional potential of pyrrole oligomers was performed by Millefiori and Alparone [22]. In another earlier study [23], density functional theoretic (DFT) calculations including configuration interaction (CI) were carried out to investigate the pathways of the unimolecular isomerizations of pyrrole. In this study, it was found that the potential energy surface of the overall isomerization of pyrrole is composed of pyrrolenine, two biradical intermediates, and five transition states, in addition to pyrrole and its stable isomers.

The structure and energetics of the pyrrole dimer were investigated by ab-initio calculations more than a decade ago by Park and Lee [24]. In this study the N–H hydrogen of one monomer points toward the ring plane of the other monomer with a distance 1.909 Å. This is a clear manifestation of hydrogen bond formation in aromatic–aromatic interactions and the electrostatic and charge transfer interactions play an important role in stabilizing this complex. An FT-IR study of pyrrole self association in CCl_4 solutions was carried out a few years ago by Stefov et al. [25]. In this study the IR measurements revealed that pyrrole forms self-associated dimeric species via N–H…π hydrogen bonding and this result was also confirmed by quantum chemical calculations for pyrrole monomer and dimer at B3LYP/6-31++G(d,p) level of theory. Recently pH dependent Raman study of pyrrole in aqueous medium was made by our group [26] and the assignments of all the normal modes of pyrrole were made on the basis of potential energy distribution (PED). Another recent work on characterization of guanidiniocarbonyl pyrroles in water by pH-dependent UV Raman spectroscopy and component analysis was reported by Srivastava et al. [27]. Most recently Barbatti et al. [28] reported the non-adiabatic dynamics simulations for pyrrole employing time-dependent density functional theory (TD-DFT) using the trajectory surface hopping approach and in this work the predominance of the N–H stretch mechanism for excited state relaxation was shown.

Since pyrrole is a heterocyclic aromatic ring that serves as a basic building block for important biomolecules, the study on the pattern of its complex formation is expected to provide information relevant to the aromatic–solvent interactions which take place widely in biological systems. In view of this fact as well as the foregoing discussion a systematic concentration dependent Raman study of the reference molecule pyrrole (C_4H_5N) in a solvent dichloromethane (DCM, CH_2Cl_2) seems to be desirable. Therefore, the present study was undertaken with an objective to examine the intermolecular interaction between the pyrrole molecule and the solvent, DCM to monitor the influence of hydrogen bonding on spectral features and to model the hydrogen bonding patterns between the reference molecule pyrrole and the solvent, DCM.

Experimental details

Pyrrole and DCM obtained from Fluka were used after distillation. The samples were stored in an N_2-atmosphere after opening in order to avoid any contamination from the surrounding atmosphere. The 275 nm line from an Ar^+- ion laser (Spectra Physics, model BeamLok 2085) was used for the Raman measurements. The laser power at the sample was ~50 mW. The reason for choosing UV excitation line is the occurrence of strong fluorescence from Pyrrole with visible excitation (514.5 nm). On the other hand it is also advantageous to use higher frequency of UV laser because the Raman intensity obtained by UV excitation line is much higher than that obtained by NIR or visible line excitation [29–32]. Raman spectra were recorded employing a 90° scattering geometry using a rotating quartz cuvette in order to avoid photochemical decomposition. The scattered light was focused on to the entrance slit of a double monochromator (Spex, model 1404 with 2400 grooves mm^{-1} holographic gratings) and the signal was detected using a liquid N_2- cooled CCD camera (Photometrics, model SDS 9000). Raman spectra were recorded using the data acquisition technique in the scanning multichannel mode employing a two-fold spectral overlap. The integration time was ~3–4 min per spectral window. The dimethylsulfoxide (DMSO) was used as a standard and its Raman peaks were used for wavenumber calibration.

Computational details

All the theoretical calculations were performed using Gaussian 03 program package [33]. The geometrical structures and the input parameters for the geometry optimization and the frequency calculations were made using GaussView03

program [34]. The optimized gas phase geometrical structures and vibrational wavenumbers of the pyrrole molecule and its HB complex with DCM were calculated using ab-initio (HF and MP2) and density functional theory (DFT) using the hybrid functional that mixes the Lee, Yang and Parr functional for the exchange correlation (B3LYP) [35, 36]. The high level basis set 6-311++G(d,p) [37] was employed for all the calculations. In some of our recent studies [18, 19, 26, 38–41] also we performed DFT calculations using B3LYP functional with the high level basis set 6-311++G(d,p) and this was quite helpful to interpret the experimental results meaningfully. Apart from the gas phase calculation, we also calculated the solvated structures of pyrrole. However, the optimized gas phase structures were given as the input geometries. The polarizable continuum model (PCM) [42] was used for the bulk solvent effect. However, in one of the studies made by Mennucci et al. [43], it has been reported that the PCM method is incapable of simulating the nonelectrostatic effects of carbon tetrachloride, benzene, and chloroform. In our study the solvent DCM is very similar to chloroform but has one more Cl atom, where nonelectrostatic effects are less pronounced we performed PCM (specific plus bulk) solvent effect or explicit solvation [44] calculations in order to explain the experimental results. All the calculations were performed without applying any constraints. All the optimized structures finally converged to the minimum of the potential surface which was inferred from the absence of negative (imaginary) wavenumber for any normal mode.

Results and discussion

Experimental results and spectral analysis

The Raman spectra of neat pyrrole and nine other binary mixtures of (pyrrole + DCM) with mole fraction of pyrrole, C=0.9, 0.8, 0.7, 0.6, 0.5, 0.4, 0.3, 0.2 and 0.1, in the region 600–1600 cm^{-1}, are presented in Fig. 1. A non-linear curve fitting was made for the spectra recorded at all concentrations with standard software *SpectraCalc*. A rigorous line shape analysis was performed for the spectra recorded at each concentration in the region 600 – 1600 cm^{-1}. The fitting procedure was carried out taking each component band as a mixture of Lorentzian and Gaussian lineshapes, which is essentially as good as a Voigt profile [45]. In order to check the uniqueness of the fitting parameters thus obtained, each spectrum was fitted with several varying, but reasonable initial guesses and each guess yielded the same fitting parameters and fitted profiles. After the rigorous analysis the precise values of the spectral parameters, peak positions, linewidths and their relative intensities were obtained for the spectra at each mole fraction of pyrrole in the binary mixtures (pyrrole + DCM). The lineshape

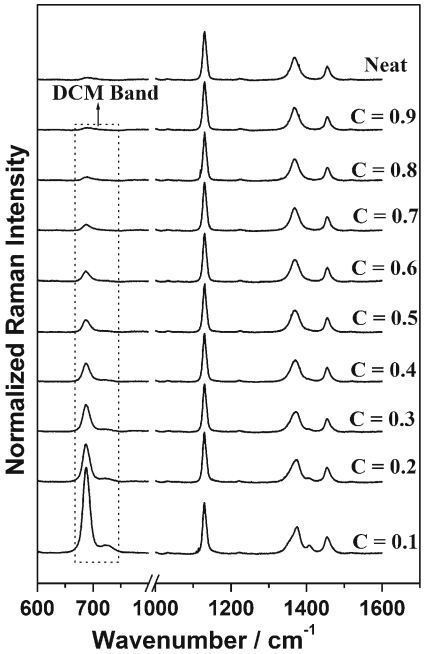

Fig. 1 Raman spectra of neat pyrrole and nine other binary mixtures (pyrrole + DCM) with mole fractions of pyrrole, C=0.9, 0.8, 0.7, 0.6, 0.5, 0.4, 0.3, 0.2 and 0.1 in the range 600-1600 cm^{-1}

analysis confirmed that only a ~1369 cm^{-1} band, which was assigned to a ring vibration of the pyrrole [26], shows a significant change in its peak position upon solvation with DCM. The band at ~688 cm^{-1} with increasing Raman intensity upon dilution in the binary mixtures (pyrrole + DCM), corresponds to avibrational band of DCM.

In order to make a clear presentation of the affected band, analyzed component bands in the region 1300 – 1500 cm^{-1} at seven different mole fraction of pyrrole, C=1.0, 0.8, 0.6, 0.5, 0.4, 0.2 and 0.1 are presented in Fig. 2 and the corresponding spectral parameters are reported in Table 1. A close examination of the spectra in the region, 1300 – 1500 cm^{-1} (see Fig. 2) revealed that a new band starts appearing at ~1351 cm^{-1} on the lower wavenumber side of the ~1369 cm^{-1} band at C=0.4. It is interesting to note that the intensity of this newly developed band goes on increasing upon dilution, which leads to the conclusion that the new band arises due to the formation of a HB species between pyrrole and DCM. In some of our earlier studies [19, 38, 40] also a new band was observed on lower or higher wavenumber side of the marker Raman band due to hydrogen bonding interaction. The plot between mole fraction of pyrrole vs. intensity ratio (I_{HB} / I_{main}) is presented in Fig. 3, which clearly shows that the intensity of the new band goes on increasing with dilution and this increase in intensity takes place at the cost of loss in intensity of the main band at ~1369 cm^{-1}. This further confirms that the newly developed band at ~1351 cm^{-1} is essentially due to HB species, which may be attributed to the fact that the DCM molecule gets attached to the pyrrole molecule in such a way that only ring

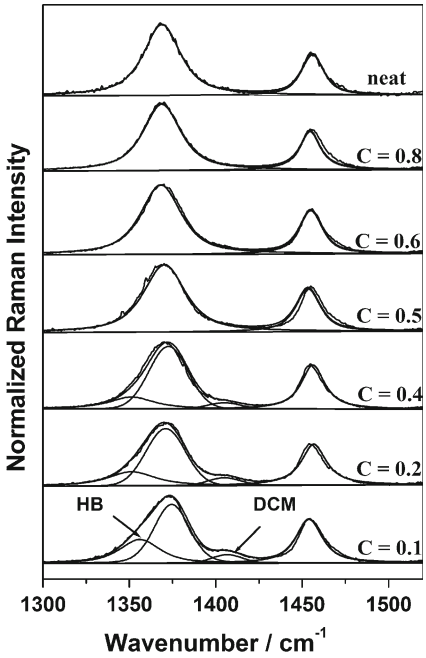

Fig. 2 Analyzed component bands corresponding to ~1369 cm^{-1} band of neat pyrrole and seven other binary mixtures (pyrrole + DCM) with mole fractions of pyrrole, C=0.8, 0.6, 0.5, 0.4, 0.2, and 0.1 in the range 1300-1500 cm^{-1}

vibration of the pyrrole molecule is significantly affected. This aspect shall be discussed in terms of the calculated optimized structures in the forthcoming section.

Theoretical results

Geometrical structures and optimized energies

The ground state optimized structures of pyrrole molecule as well as its HB complexes with one DCM molecule in two configurations, named as first and second configuration and with two DCM molecules in only one configuration obtained using the B3LYP method with highest level basis set 6-311++G(d,p) in gas phase are presented in Fig. 4. In addition to this, we have also optimized all these structures using MP2 and HF methods also employing the same basis set for the sake of comparison with the experimental results. The numbering scheme used for describing the structural parameters is presented in Fig. 4a. The calculated structural parameters: bond lengths, bond angles and dihedral angles of neat pyrrole in gas phase using ab-initio methods HF, MP2 and DFT method employing B3LYP functional match very well with the experimental data [46, 47] and the results are reported in Table 2. The results obtained by B3LYP/6-311++G(d,p) method show a better correlation between observed and calculated parameters in comparison to those obtained by HF and MP2 methods.

In the first configuration of the complex (pyrrole + DCM), where the Cl1 and Cl2 atoms of DCM molecule are attached to H1 atom of pyrrole molecule as obtained from the gas phase calculation (see Fig. 4b), two relatively weaker hydrogen bonds (Cl1·····H1 – N1 and Cl2·····H1 – N1) were formed and the corresponding hydrogen bond lengths were calculated to be 3.07 and 3.08 Å, respectively. However, in the second configuration of the complex, the DCM molecule is attached to the π-ring of the pyrrole molecule (see Fig. 4c), whose distance was calculated to be ~2.54 Å, which essentially means that the strength of hydrogen bond is more in the case of this complex in second configuration. It is expected that the attachment of the DCM molecule to the π-ring of the pyrrole molecule will affect the ring vibration of pyrrole, which was also observed in our Raman measurements. This shows that the second configuration of the complex (pyrrole + DCM) is more favorable.

Table 1 Wavenumber positions and linewidths of the Raman peaks obtained by analyzing the observed Raman line profile in the region, 1300-1500 cm^{-1} at different mole fractions, of pyrrole, C in the binary mixtures (pyrrole + DCM)

Mole fraction (C) of pyrrole	Peak1 HB		Peak2		Peak3 (DCM)		Peak4	
	ν (cm^{-1})	Γ_{FWHM} (cm^{-1})	ν (cm^{-1})	Γ_{FWHM} (cm^{-1})	ν (cm^{-1})	Γ_{FWHM} (cm^{-1})	ν (cm^{-1})	Γ_{FWHM} (cm^{-1})
1.0	——	——	1368.8	25.7	——	——	1455.9	15.6
0.9	——	——	1368.9	25.8	——	——	1455.1	15.9
0.8	——	——	1368.9	25.9	——	——	1454.6	16.4
0.7	——	——	1368.8	27.0	——	——	1455.7	15.8
0.6	——	——	1368.8	28.1	——	——	1455.0	16.0
0.5	——	——	1370.4	29.0	——	——	1453.5	17.1
0.4	1351.3	30.3	1372.6	28.1	1405.1	23.0	1456.3	16.5
0.3	1351.3	32.6	1373.0	27.3	1405.1	22.8	1456.8	17.5
0.2	1351.4	33.1	1374.3	25.7	1405.7	22.2	1456.7	19.6
0.1	1355.9	34.0	1374.5	24.5	1406.6	21.1	1454.0	18.3

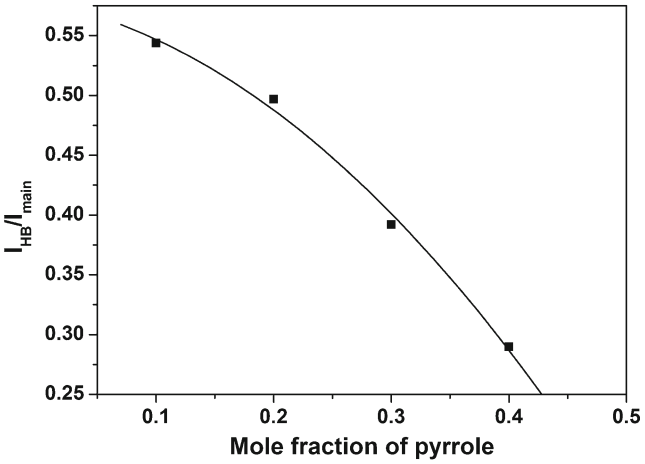

Fig. 3 Variation of the ratio of integrated intensities of the band associated to the HB species vs. ~1369 cm^{-1} band (I_{HB} / I_{main}) with concentration, C (0.4 to 0.1)

It is interesting to note that the MP2/6-311++G(d,p) method always optimizes the complex (pyrrole + DCM) only in second configuration, irrespective of the initial input (either in first or second configuration). However, with the B3LYP and HF methods both configurations are optimized. All the structural parameters: bond lengths, bond angles and dihedral angels of pyrrole solvated in solvent DCM using ab-initio (HF and MP2) and DFT methods using different solvation models (PCM bulk and specific plus bulk) are reported in Table 3. It is evident from the calculated structural parameters using B3LYP method that r (N1–C2), r(C2–C3), r(C4–C5), r(N1–C5) and r(H1–N1) bond lengths show changes of 0.001 Å in going from neat pyrrole to (pyrrole + 1 DCM) complex, whereas, r(C3–C4), r(H1–C2), r (H2–C2), r(H3–C3), r(H4–C4) and r(H5–C5) bond lengths do not show any change. However, PCM (bulk) and PCM (specific plus bulk) solvations show significant changes in all the above mentioned parameters of pyrrole upon complexation. The solvation with PCM (bulk) and PCM (specific plus bulk) solvation show almost the same results. The angles ∠H2C3N1 and ∠H3C3C2 show slight change of 0.1^0 upon complexation with DCM. However, other angles do not show any change in comparison to gas phase calculations. MP2 and HF methods also show similar trends for all the parameters as DFT method.

Since the structure of (pyrrole + 1 DCM) in second configuration was found to be most favored according to our experimental observation, we have also optimized the (pyrrole + 2 DCM) in second configuration for the sake of comparison with the experimental results, especially at high dilutions. In this configuration the H7 and H7' atoms of two different DCM molecules are attached to the π-ring of the pyrrole through hydrogen bonds (see Fig. 4d). The separation of the hydrogen atoms H7 and H7' of the DCM from the center of the π-ring of pyrrole was calculated to be 2.64 Å. All the parameters related to (pyrrole + 2 DCM) in second configuration are also reported in Table 3.

The ground state energies of isolated pyrrole and its HB complexes with one and two DCM molecules, in both gas phase and PCM solvation, at different levels of theories (B3LYP, MP2 and HF) are presented in Table 4. The effect of the basis set super position error (BSSE) correction was also incorporated in the optimized structures of the complexes by the standard counterpoise method [48, 49] and the BSSE corrected optimized energies are also presented in Table 4. The binding energy of the complex is defined as usual by:

$$\Delta E = \left[E_{complex} - \left(E_{pyrrole} + nE_{DCM}\right)\right] + E_{BSSE}, \quad (1)$$

where n is the number of DCM molecules.

The binding energies of (pyrrole + 1 DCM) in first and second configurations and (pyrrole + 2 DCM) in second configuration using the above equation were obtained to be 2.26, 3.26 and 3.30 kcal mol^{-1} per DCM molecule using B3LYP/6-311++G(d,p) method and the corresponding values using the HF method were calculated to be 2.26, 3.45 and 3.20 kcal mol^{-1}. The binding energies of (pyrrole + 1 DCM) and (pyrrole + 2 DCM) in the second configuration using the above equation were obtained to be 2.07 and 3.19 kcal mol^{-1}, respectively using MP2/6-311++G(d,p) method. Thus on the basis of calculated total binding energies (pyrrole + 1 DCM) in second configuration (where DCM molecule is attached to the π-ring of the pyrrole molecule) is most stable.

Correlation of experimental and theoretical results

Since the calculated harmonic vibrational wavenumbers overestimate the observed anharmonic vibrational wavenumber [33], we scaled all the calculated wavenumbers with the experimental value. The scaling of the theoretically calculated Raman modes was made with respect to the intense Raman band at ~1139 cm^{-1}. The scaling factors for the B3LYP, MP2 and HF methods were calculated to be 0.9653, 0.9614 and 0.9042, respectively. A nice agreement between the experimentally measured and calculated scaled wavenumbers of the normal modes at different levels of theory is presented in Fig. 5. These scaling factors are quite close to the standard scaling factor [50]. In order to show the relative agreement between the experimental and calculated parameters, we calculated the root mean square deviation of the calculated structural parameters with reference to the experimental values Ref. [46] given in Table 2. The values of the root mean square deviation for the B3LYP, MP2 and HF methods were found to be 0.1710, 0.2254 and 0.2661, respectively. This statistical analysis shows that the B3LYP method gives a nice agreement with the experimental value [18, 39, 41] as compared to the MP2 and HF results.

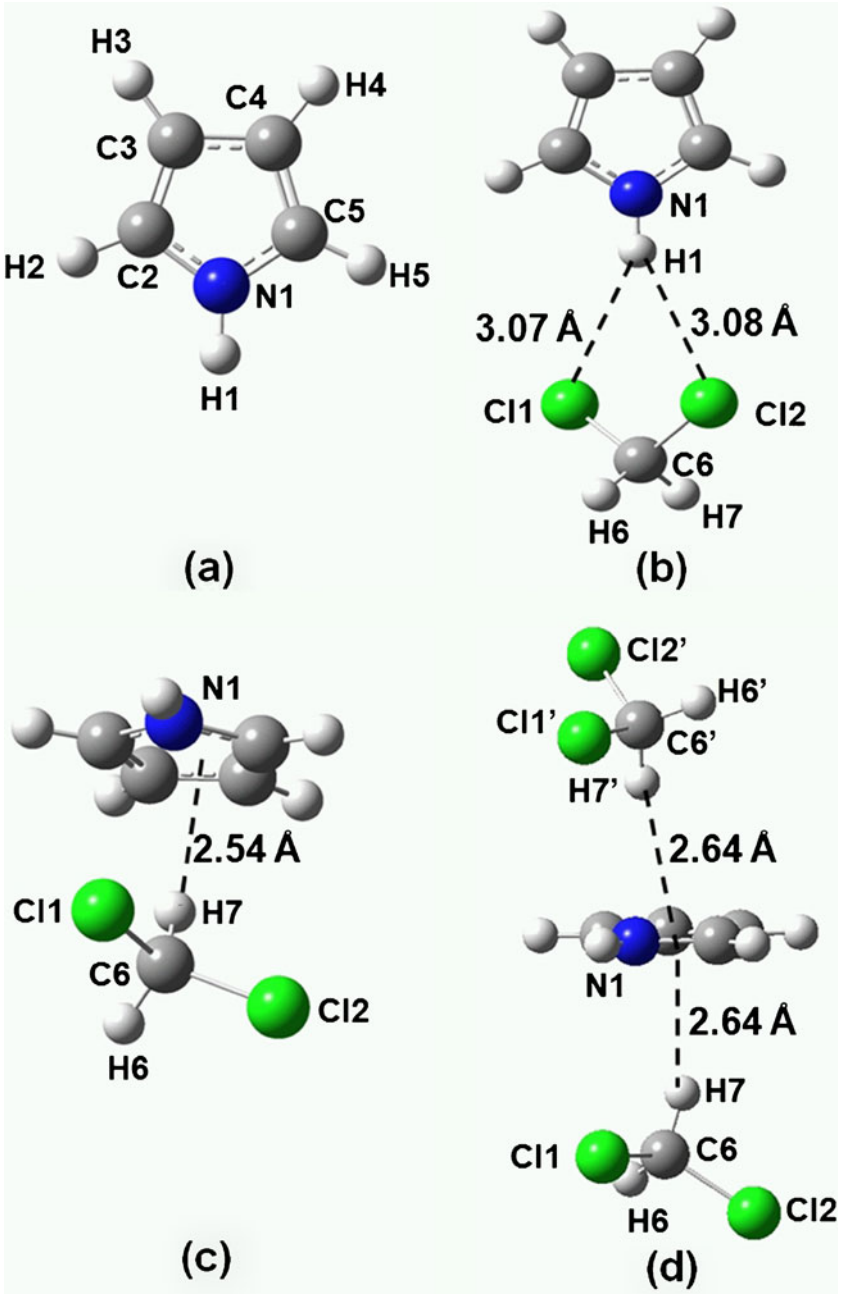

Fig. 4 Optimized geometries of neat pyrrole and its complex with one and two DCM molecules using B3LYP/6-311++G(d,p) level of theory in gas phase: **(a)** neat pyrrole; **(b)** N-H of pyrrole molecule bonded to the Cl atom of DCM molecule (first configuration); **(c)** H atom of DCM molecule bonded to π ring of the pyrrole molecule (second configuration); **(d)** H atom of both DCM molecules bonded to π ring of the pyrrole molecule (second configuration)

Further, it is to be noted that the quantum chemical calculations yield Raman activities for the different normal modes, which cannot be taken directly as Raman intensities. The Raman scattering cross sections, $\partial\sigma/\partial\Omega$, which are proportional to the Raman intensities, may be calculated from the Raman scattering amplitude and predicted wavenumber for each normal mode using the following relationship [51, 52]:

$$\frac{\partial\sigma_j}{\partial\Omega} = \left(\frac{2^4\pi^4}{45}\right)\left(\frac{(\nu_0-\nu_j)^4}{1-\exp\left[\frac{-hc\nu_j}{kT}\right]}\right)\left(\frac{h}{8\pi^2 c\nu_j}\right)S_j, \qquad (2)$$

where, ν_0 is the exciting frequency, ν_j is the vibrational frequency of the jth normal mode, S_j is the corresponding Raman scattering amplitude obtained from the DFT calculations and h, c and k are the universal constants. The Raman intensities obtained using this relationship match nicely with the experimentally observed intensities.

The experimentally observed Raman spectra of highly diluted pyrrole (C<0.1) with DCM and calculated scaled Raman spectra of complexes of pyrrole with one DCM molecule in gas phase as well as in solvation (Bulk and specific plus bulk) in the region 600-1600 cm^{-1} are presented in Fig. 6. The band at ~1405 cm^{-1} which corresponds to the vibration of DCM molecule has been observed both in theoretically calculated as well as in the experimentally recorded spectra. A new band (~1351 cm^{-1}) is also observed

Table 2 Calculated structural parameters: bond lengths, bond angles and dihedral angles for neat pyrrole in gas phase using ab-initio methods, HF, MP2 and DFT method employing B3LYP functional

	$(Pyrrole)_{gas}$				
	Experimental		B3LYP	MP2	HF
	Ref. 46	Ref. 46	6-311++G(d,p)	6-311++G(d,p)	6-311++G(d,p)
Bond length (Å)					
r(N1-C2)	1.370	1.390	1.375	1.374	1.363
r(C2-C3)	1.382	1.380	1.377	1.388	1.359
r(C3-C4)	1.417	1.410	1.425	1.423	1.428
r(C4-C5)	——	——	1.377	1.388	1.359
r(N1-C5)	——	——	1.375	1.374	1.363
r(H1-N1)	0.996	1.010	1.006	1.009	0.991
r(H1-C2)	——	——	2.120	2.119	2.010
r(H2-C2)	1.076	1.070	1.078	1.080	1.070
r(H3-C3)	1.077	1.080	1.079	1.081	1.071
r(H4-C4)	——	——	1.079	1.081	1.071
r(H5-C5)	——	——	1.078	1.080	1.070
Bond angle					
∠(C2N1C5)	109.8	109.7	109.8	110.2	109.5
∠ (N1C2C3)	107.7	107.4	107.7	107.5	108.2
∠ (C2C3C4)	107.4	108.0	107.4	107.4	107.1
∠ (C3C4C5)	——	——	107.4	107.4	107.1
∠ (C4C5N1)	——	——	107.7	107.5	108.2
∠ (H1N1C2)	125.1	——	125.1	124.9	125.3
∠ (H2C2N1)	120.8	——	121.3	121.2	121.3
∠ (H2C2C3)	130.8	——	131.1	131.3	130.6
∠ (H3C3C2)	125.5	——	125.7	125.6	125.9
Dihedral angle					
τ (H1C2C3C4)	——	——	-0.01	0	-0.04
τ (H2C2C3C4)	——	——	180.0	180	180
τ (N1C5C4C3)	——	——	0	0	-0.06
τ (H5C5C4C3)	——	——	180.0	180.0	180.0

The atom numbering is shown in Fig. 4

as a side band on lower wavenumber side of ring vibration (~1369 cm^{-1}) which is essentially due to weak interaction between pyrrole and DCM.

The experimentally measured peak position for neat pyrrole and its HB complexes with DCM at high dilution (C<0.1), the wavenumber shift, corresponding to calculated (only B3LYP) unscaled peak positions of neat pyrrole in gas phase and its complexes with one / two DCM molecules in gas phase as well as in solvation with DCM are presented in Table 5 for comparison. The peak at ~1369 cm^{-1} corresponding to ring vibration shows a significant shift (~6 cm^{-1}) upon dilution with DCM. However, when we compared the corresponding bands in theoretical calculationsm we find that (pyrrole + 2 DCM) shows a significant shift in going from neat to the HB complex (Fig. 4c). This aspect was common in both gas phase as well as specific plus bulk solvation calculation. Thus, it was observed that both the gas phase and PCM (specific plus bulk) solvation effect show a reasonably good agreement with the experimental results (see Fig. 6).

Line shape analysis of the Raman band at ~1369 cm^{-1} (ring vibration) in the binary mixture ($C_4H_5N + CH_2Cl_2$)

In the Raman spectra presented in Fig. 2, the band at ~1369 cm^{-1} shows a composite peak nature upon dilution with DCM. This band was analyzed to two peaks at high dilution (C< 0.4), which are referred to as peak 1 (HB) and peak 2 (ring vibration of pyrrole), respectively, and are presented in Table 1. The variation of peak position and the linewidth with concentration for the analyzed band at ~1369 cm^{-1} is presented in Fig. 7. It is obvious from the data presented in Fig. 7 that peak 2 shows a significant blue shift (~6 cm^{-1}) in going from neat pyrrole to extreme dilution. However, the shift does not follow

Table 3 Calculated structural parameters: bond lengths, bond angles and dihedral angles of pyrrole solvated in the solvent DCM using ab-initio methods (HF and MP2) and DFT method employing B3LYP functional using different solvation models

Structural parameters	B3LYP			MP2			HF		
	6-311++G(d,p)			6-311++G(d,p)			6-311++G(d,p)		
	$(Solv)_{gas}$	$(Solv)_B$	$(Solv)_{SB}$	$(Solv)_{gas}$	$(Solv)_B$	$(Solv)_{SB}$	$(Solv)_{gas}$	$(Solv)_B$	$(Solv)_{SB}$
Bond length (Å)									
r(N1-C2)	1.374	1.373	1.374	——	1.372	——	1.362	1.361	1.362
	(1.375)		(1.373)	(1.374)		(1.373)	(1.363)		(1.361)
	[1.374]		[1.374]	[1.372]		[1.371]	[1.362]		[1.360]
r(C2-C3)	1.378	1.38	1.380	——	1.391	——	1.359	1.363	1.362
	(1378)		(1.381)	(1.389)		(1.391)	(1.360)		(1.363)
	[1.379]		[1.381]	[1.391]		[1.392]	[1.361]		[1.364]
r(C3-C4)	1.425	1.427	1.427	——	1.425	——	1.428	1.429	1.430
	(1.425)		(1.427)	(1.425)		(1.428)	(1.428)		(1.429)
	[1.425]		[1.427]	[1.425]		[1.428]	[1.428]		[1.429]
r(C4-C5)	1.378	1.38	1.380	——	1.391	——	1.359	1.363	1.362
	(1378)		(1.381)	(1.389)		(1.391)	(1.360)		(1.363)
	[1.379]		[1.381]	[1.390]		[1.392]	[1.361]		[1.364]
r(N1-C5)	1.374	1.373	1.374	——	1.372	——	1.362	1.361	1.362
	(1.375)		(1.373)	(1.374)		(1.371)	(1.363)		(1.361)
	[1.374]		[1.374]	[1.372]		[1.369]	[1.362]		[1.360]
r(H1-N1)	1.007	1.019	1.008	——	1.022	——	0.992	1.002	0.993
	(1.007)		(1.009)	(1.010)		(1.011)	(0.992)		(1.003)
	[1.007]		[1.008]	[1.011]		[1.013]	[0.992]		[1.002]
r(H1-C2)	2.120	2.128	2.120	——	2.129	——	2.097	2.104	2.097
	(2.120)		(2.119)	(2.119)		(2.117)	(2.098)		(2.104)
	[2.120]		[2.120]	[2.118]		[2.115]	[2.098]		[2.103]
r(H2-C2)	1.078	1.081	1.081	——	1.084	——	1.070	1.072	1.073
	(1.078)		(1.081)	(1.080)		(1.082)	(1.070)		(1.073)
	[1.078]		[1.081]	[1.080]		[1.082]	[1.070]		[1.073]
r(H3-C3)	1.079	1.082	1.082	——	1.084	——	1.071	1.074	1.074
	(1.079)		(1.082)	(1.081)		(1.083)	(1.070)		(1.074)
	[1.079]		[1.082]	[1.082]		[1.083]	[1.071]		[1.074]
r(H4-C4)	1.079	1.082	1.082	——	1.084	——	1.071	1.074	1.074
	(1.079)		(1.082)	(1.080)		(1.082)	(1.071)		(1.074)
	[1.079]		[1.082]	[1.081]		[1.083]	[1.071]		[1.074]
r(H5-C5)	1.078	1.081	1.081	——	1.084	——	1.07	1.073	1.073
	(1.078)		(1.081)	(1.080)		(1.082)	(1.070)		(1.073)
	[1.078]		[1.081]	[1.080]		[1.082]	[1.070]		[1.073]
r(H1-C11)	3.070	——	3.030	——	——	——	3.220	——	3.220
	(3.430)		(4.210)	(3.470)		(4.240)	(5.290)		(5.670)
	[3.520]		[3.880]	[3.520]		[4.290]	[3.740]		[5.740]
r(H1-C2)	3.080	——	3.040	——	——	——	3.250	——	3.250
	(3.430)		(4.210)	(3.570)		(4.260)	(3.720)		(4.220)
	[5.330]		[5.670]	[3.450]		[4.150]	[5.290]		[5.240]
Bond angles									
∠(C2N1C5)	109.8	109.9	109.9	——	110.3	——	109.5	109.6	109.7
	(109.8)		(109.9)	(110.3)		(110.3)	(109.6)		(119.7)
	[109.9]		[110.0]	[110.5]		[110.3]	[109.6]		[109.6]
∠(N1C2C3)	107.7	107.7	107.7	——	107.6	——	108.2	108.2	108.1
	(107.6)		(107.7)	(107.4)		(107.5)	(108.1)		(108.2)

Table 3 (continued)

Structural parameters	B3LYP			MP2			HF		
	6-311++G(d,p)			6-311++G(d,p)			6-311++G(d,p)		
	$(Solv)_{gas}$	$(Solv)_B$	$(Solv)_{SB}$	$(Solv)_{gas}$	$(Solv)_B$	$(Solv)_{SB}$	$(Solv)_{gas}$	$(Solv)_B$	$(Solv)_{SB}$
	[107.6]		[107.6]	[107.3]		[107.5]	[108.1]		[108.3]
∠ (C2C3C4)	107.4	107.3	107.4	——	107.3	——	107	107.0	107
	(107.4)		(107.3)	(107.4)		(107.3)	(107.1)		(107.0)
	[107.4]		[107.4]	[107.4]		[107.3]	[108.1]		[107.1]
∠ (C3C4C5)	107.4	107.3	107.4	——	107.3	——	107.0	107.0	107.0
	(107.4)		(107.3)	(107.4)		(107.3)	(107.1)		(107.0)
	[107.4]		[107.4]	[107.3]		[107.2]	[108.1]		[107.2]
∠(C4C5N1)	107.7	107.7	107.7	——	107.6	——	108.2	108.2	108.1
	(107.7)		(107.8)	(107.4)		(107.3)	(108.1)		(108.2)
	[107.6]		[107.8]	[107.4]		[107.3]	[108.1]		[108.3]
∠(H1N1C2)	125.1	125.1	125	——	124.9	——	125.3	125.2	125.1
	(125.1)		(125.0)	(124.8)		(125.6)	(125.2)		(125.1)
	[125.0]		[124.8]	[124.7]		[125.4]	[125.2]		[125.1]
∠(H2C2N1)	121.2	121.1	121.2	——	121.1	——	121.2	121.1	121.2
	(121.3)		(121.1)	(121.2)		(121.1)	(121.3)		(121.1)
	[121.2]		[121.2]	[121.2]		[121.3]	[121.2]		[121.2]
∠(H2C2C3)	131.1	131.1	131.2	——	131.4	——	130.6	130.6	130.7
	(131.1)		(131.1)	(131.1)		(131.2)	(130.6)		(130.7)
	[131.1]		[131.2]	[131.4]		[131.4]	[130.6]		[130.8]
∠(H3C3C2)	125.8	125.8	125.7	——	125.6	——	125.9	126	125.9
	(125.7)		(125.8)	(125.5)		(125.7)	(125.9)		(126.0)
	[125.7]		[125.7]	[125.5]		[125.8]	[125.9]		[125.8]
∠(N1H1C11)	151.3	——	150.8	——	——	——	154.8	——	154.8
	(74.8)		(54.5)	(86.8)		(59.8)	(69.8)		(57.7)
	[95.4]		[95.6]	[84.9]		[85.1]	[93.4]		[82.1]
∠(N1H1C12)	150.7	——	150.3	——	——	——	151	——	151
	(97.7)		(89.4)	(86.8)		(59.8)	(94.3)		(85.8)
	[67.4]		[67.7]	[84.8]		[84.9]	[69.2]		[63.1]
∠(N1H7C6)	(137.4)	——	(148.3)	(121.7)	——	(134.7)	(142.1)	——	(149.1)
	[137.1]		[148.1]	[119.1]		[119.3]	[142.1]		[144.8]
Dihedral angles									
τ(H1C2C3C4)	0	-0.3	0	——	-0.01	——	-0.01	0	-0.01
	(1.30)		(-0.13)		(1.87)		(-0.24)	(0.75)	(-0.07)
	[0.15]		[0.18]		[-0.02]		[-0.07]	[0.06]	[-0.09]
τ (H2C2C3C4)	-180	179.9	179.9	——	180	——	180	180	179.9
	(179.7)		(179.8)		(179.7)		(179.8)	(179.8)	(179.9)
	[180.0]		[179.9]		[179.7]		[179.9]	[179.9]	[179.9]
τ (N1C5C4C3)	0	-0.01	0.01	——	0	——	-0.02	0	-0.03
	(0.14)		(-0.02)		(0.08)		(-0.07)	(-0.02)	(-0.04)
	[0.10]		[0.14]		[-0.34]		[-0.11]	[0.07]	[-0.09]
τ (H5C5C4C3)	-180	179.9	179.9	——	-180	——	180	179.9	179.9
	(-179.8		(179.9)		(-179.8)		(179.9)	(179.8)	(179.9)
	[179.9]		[180.0]		[179.7]		[179.9]	[179.9]	[179.9]

The atom numbering is shown in Fig. 4. $(Solv)_{gas}$- Solvation in gas phase; $(Solv)_B$- Bulk solvation; $(Solv)_{SB}$- Specific plus bulk solvation. The parameters presented in parentheses ( ) and [ ] denote the value in second configuration with one and two DCM molecules, respectively

Table 4 Optimized ground state total energies (au) of pyrrole and its complexes with one DCM and two DCM obtained at the B3LYP, MP2 and HF/6-311++G(d,p) levels of theory in gas phase, PCM (bulk) and PCM (specific plus bulk)

	Optimized energies			
	Gas phase	BSSE corrected value (Gas phase)	PCM (Bulk solvation)	PCM (Specific plus bulk solvation)
B3LYP				
Pyrrole (neat)	-210.2306	——	-210.2414	——
DCM (neat)	-959.7682	——	——	——
Pyrrole + 1 DCM (I^{st} Confg.)	-1170.0015	-1170.0006	——	-1170.0111
Pyrrole + 1 DCM (II^{nd} Confg.)	-1170.0030	-1170.0020	——	-1170.0149
Pyrrole + 2 DCM (II^{nd} Confg.)	-2129.7752	-2129.7729	——	-2129.7967
MP2				
Pyrrole (neat)	-208.8623	——	-209.6131	——
DCM (neat)	-958.0511	——	——	——
Pyrrole + 1 DCM (I^{st} Confg.)	——	——	——	——
Pyrrole + 1 DCM (II^{nd} Confg.)	-1166.9155	-1166.9122	——	-1166.9240
Pyrrole + 2 DCM (II^{nd} Confg.)	-2126.5892	-2126.5841	——	-2126.6113
HF				
Pyrrole (neat)	-208.8646	——	-208.8758	——
DCM (neat)	-958.0504	——	——	——
Pyrrole + 1 DCM (I^{st} Confg.)	-1166.9177	-1166.9168	——	-1166.9283
Pyrrole + 1 DCM (II^{nd} Confg.)	-1166.9194	-1166.9183	——	-1166.9319
Pyrrole + 2 DCM (II^{nd} Confg.)	-2124.9736	-2124.9716	——	-2124.9947

the linear trend. Peak 1 does not show any significant change in its peak position upto C=0.6 mole fraction of pyrrole, but at intermediate concentration, C=0.5 it shows sudden upshift of ~1.6 cm^{-1} and beyond this point a continuous increment is observed. When we look at the trend of concentration dependent linewidth variation of this band, it shows an increase in linewidth upon dilution initially by ~3.3 cm^{-1} upto C=0.5 mole fraction, and in going below C=0.6 it starts decreasing on further dilution (see Table 1). The spectral changes

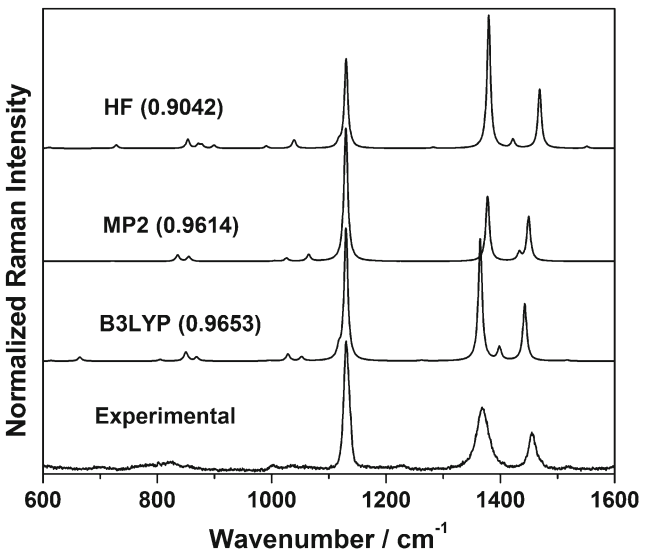

Fig. 5 The comparison between the experimentally measured and calculated scaled Raman spectra of neat pyrrole using the methods, B3LYP, MP2 and HF, respectively (from lower to upper) in the region 600–1600 cm^{-1}

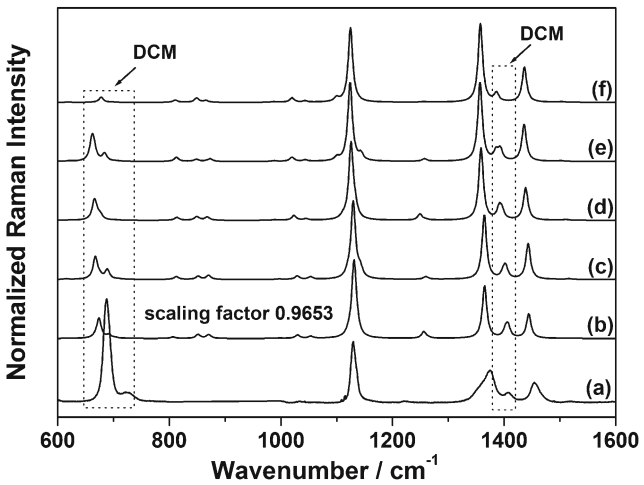

Fig. 6 Raman spectra of pyrrole with DCM: (**a**) experimental (C<0.1) (**b**)/(**c**) calculated scaled spectra of pyrrole with one DCM molecule in gas phase of first configuration/second configuration, (**d**)/(**e**) complex with one DCM molecule in PCM (specific plus bulk solvation) of first configuration/second configuration, (**f**) using PCM solvation (bulk effect)

Table 5 Experimentally measured wavenumber positions of the vibrational bands of neat pyrrole, pyrrole + DCM, shifts and calculated scaled wavenumber positions of both configuration in gas phase and solvated pyrrole (gas phase, bulk solvation and specific plus bulk solvation using PCM) at B3LYP level

Experimental			Theoretical (B3LYP)							
			Gas phase				Solvation			
Py	Py + DCM	$\Delta\nu_{exp}$	Py_{neat}	(Py + 1DCM) I^{st} Confg.	(Py + 1DCM) II^{nd} Confg.	(Py + 2DCM) II^{nd} Confg.	Py B.sol	(Py + 1DCM)SB.sol I^{st} Confg.	(Py + 1DCM)SB.sol II^{nd} Confg.	(Py + 2DCM)SB.sol II^{nd} Confg.
825	826	+1	810	807	810	814	810	815	811	816
1001	1002	+1	1027	1030	1030	1032	1020	1026	1020	1023
1037	1037	0	1052	1054	1054	1066	1054	1056	1048	1061
1130	1131	+1	1129	1131	1132	1170	1125	1128	1125	1163
1369	1375	+6	1364	1367	1367	1412	1357	1358	1359	1409
1456	1457	+1	1442	1444	1445	1451	1437	1438	1437	1441

B.sol.- Bulk solvation; SB.sol.- Specific plus Bulk solvation

observed for this band are similar to what one would expect from the the concentration fluctuation model of Bondarev and Mardaeva, [53] which gives a maximum around C=0.5 in the linewidth vs. concentration plot and this concentration fluctuation seems to play a major role in this case. The diffusion mechanism, as discussed in our earlier study [41] on paraldehyde, is basically caused due to more and more solvent molecules colliding with a reference molecule causing a decrease in T_2 lifetime [54] and thereby causing a line broadening. In this case it seems that the concentration fluctuation plays a dominant role, which apparently causes maxima at a concentration of C=0.5 of the reference system, pyrrole and diffusion seems to be less important.

The peak corresponding to the HB complex (which is observed at C=0.4 and below) shows a blue shift (see Table 1), whereas this band shows ~3.7 cm^{-1} broadening upon dilution with DCM. The broadening of this peak is essentially due to fast dynamics at high dilution which essentially decreases the lifetime of the v=1 state corresponding to the HB complex, thereby leading to line broadening.

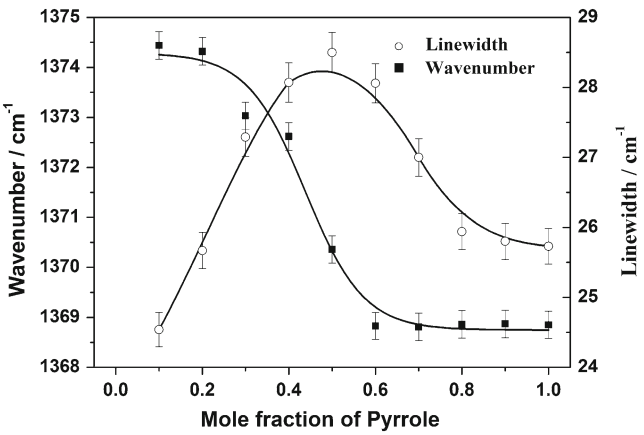

Fig. 7 Variation of peak positions and linewidths of the ~1369 cm^{-1} mode vs. concentration, C (same as in Fig. 1) in mole fraction of pyrrole in the binary mixture pyrrole + DCM

Conclusions

The present study was undertaken with an objective to examine the intermolecular interaction between the pyrrole and DCM molecule using Raman spectroscopic technique and quantum chemical calculations. The weak hydrogen bonding between the reference molecule pyrrole and the solvent, DCM was monitored by studying the influence of hydrogen bonding on spectral features. The Raman spectra in the region, 1300 – 1500 cm^{-1} (see Fig. 2) showed that a new band starts appearing at ~1351 cm^{-1} on the lower wavenumber side of the ~1369 cm^{-1} (which was assigned as ring vibration) band at C=0.4 and the intensity of this newly developed band goes on increasing upon dilution, which leads to the conclusion that the new band arises due to the formation of a hydrogen bonded species between pyrrole and DCM. In order to simulate our experimental results we have performed the ab-initio (HF and MP2) and DFT calculations. It was observed that the B3LYP and HF optimizations two stable complex structures, while MP2 method optimized only one stable complex. By looking at the binding strengths of the complexes it was observed that the complex of pyrrole and DCM in second configuration (where DCM molecule was attached to π ring of pyrrole) was generically more stable and significantly affects the ring vibrations of pyrrole. Due to higher stability of the second configuration, it is more probable that in the mixture, the species corresponding to the second configuration is larger in number, and hence shows a pronounced effect on ring vibrations of pyrrole. Overall this study presents a very good example of monitoring very weak hydrogen bonding experimentally and by modeling different structures at different levels of theory

provides a nice correlation between experimental and theoretical results.

Acknowledgments The authors would like to thank Prof. Wolfgang Kiefer and Prof. Sebastian Schlücker for providing access to their laboratory facilities to one of us (DKS) to make the Raman measurements. DKS is also thankful to the Council of Scientific and Industrial Research (CSIR), India for the award of Senior Research Fellowship (SRF). Authors are thankful to Ms. Shweta Singh for the help in preparation of the manuscript. SKS is thankful to DST for the award of DST-Fast Track Young Scientist.

References

1. Jeffrey GA (1997) An introduction to hydrogen bonding. Oxford University Press, New York
2. Scheiner S (1997) Hydrogen bonding: a theoretical perspective. Oxford University Press, Oxford
3. Wilson KR, Tobin JG, Ankudinov AL, Rehr JJ, Saykally RJ (2000) Phys Rev Lett 85:4289–4292
4. Gale GM, Gaillot G, Hache F, Lascoux N, Bratos S, Leickman J-CL (1999) Phys Rev Lett 82:1068–1071
5. Morgenstern K, Nieminen J (2002) Phys Rev Lett 88:066102–066105
6. Finney JL, Hallbrucker A, Kohl I, Soper AK, Bowron DT (2002) Phys Rev Lett 88:225503–225506
7. Kirby A (1997) J Acc Chem Res 30:290–296
8. Hobza P, Zahradnik R (1988) Intermolecular complexes. Academia, Prague
9. Pimentel GC, McClellan AL (1960) The hydrogen bond. Freeman, San Francisco
10. Asthana, BP, Kiefer W (1992) In: Durig JR (ed) Vibrational spectra and structure. Elsevier, Amsterdam, 20:67–159
11. Asthana BP, Takahashi H, Kiefer W (1983) Chem Phys Lett 94:41–47
12. Cabaco MI, Besnard M, Yarwood J (1992) Mol Phys 75:139–155
13. Singh RK, Bhriguvansh P, Asthana BP, Verma AL (1998) Chem Phys Lett 296:611–618
14. Schlücker S, Singh RK, Asthana BP, Popp J, Kiefer W (2001) J Phys Chem A 105:9983–9989
15. Zoidis E, Yarwood J, Danten Y, Besnard M (1995) Mol Phys 85:373–385
16. Deckert V, Asthana BP, Mishra PC, Kiefer W (1996) J Raman Spectrosc 27:907–913
17. Torii H, Tasumi M (1998) J Phys Chem B 102:315–321
18. Singh DK, Srivastva SK, Ojha AK, Asthana BP (2008) J Mol Struct 892:384–391
19. Singh DK, Mishra S, Ojha AK, Srivastava SK, Schlücker S, Asthana BP, Popp J, Singh RK (2011) J Raman Spectrosc 42:667–675
20. Tubergen MJ, Andrews AM, Kuczkowski RL (1993) J Phys Chem 97:7451–7457
21. Martoprawiro MA, Bacskay GB (1995) Mol Phys 85:573–585
22. Millefiori S, Alparone A (1998) J Chem Soc Faraday Trans 94:25–32
23. Dubnikova F, Lifshitz A (1998) J Phys Chem A 102:10880–10888
24. Park H, Lee S (1999) Chem Phys Lett 301:487–492
25. Stefov V, Pejov L, Soptrajanov B (2003) J Mol Struct 649:231–243
26. Singh DK, Srivastva SK, Ojha AK, Asthana BP (2008) Spectrochim Acta 71 A:823–829
27. Srivastava SK, Niebling S, Küstner B, Wich PR, Schmuck C, Schlücker S (2008) Phys Chem Chem Phys 10:6770–6775
28. Barbatti M, Pittner J, Pederzoli M, Werner U, Mitric R, Bonačić-Koutecký V, Lischka H (2010) Chem Phys 375:26–34
29. Li C, Stair PC (1997) Catal Today 33:353–366
30. Yu Y, Xiong G, Li C, Xiao F-S (2000) J Catal 194:487–490
31. Xiong G, Yu Y, Feng Z-C, Xin Q, Xiao F-S, Li C (2001) Micropor Mesopor Mater 42:317–323
32. Yu Y, Yu J-H, Xiong G, Li C, Xiao F-S (2001) Phys Chem Chem Phys 3:2692–2696
33. Frisch MJ, Trucks GW, Schlegel HB, Scuseria GE, Robb MA, Cheeseman JR, Zakrzewski VG, Montgomery JA, Stratmann RE Jr, Burant JC, Dapprich S, Millam JM, Daniels AD, Kudin KN, Strain MC, Farkas O, Tomasi J, Barone V, Cossi M, Cammy R, Mennucci B, Pomelli C, Adamo C, Clifford S, Ochterski J, Petersson GA, Ayala PY, Cui Q, Morokuma K, Rega N, Salvodar P, Dannenberg JJ, Malick DK, Rabuck AD, Raghavachari K, Foresman JB, Cioslowski J, Ortiz JV, Baboul AG, Stefanov BB, Liu G, Liashenko A, Piskorz P, Komaromi I, Gomperts R, Martin RL, Fox DJ, Keith T, Al-Laham MA, Peng CY, Nanayakkara A, Challacombe M, Gill PMW, Johnson B, Chen W, Wong MW, Andres JL, Gonzalez C, Head-Gordon M, Replogle ES, Pople JA (2003) Gaussian 03, revision B.05. Gaussian Inc, Pittsburgh
34. Dennington R II, Keith T, Millam J, Eppinnett K, Lee Hovell W, Gilliland R (2003) In: Gilliland R (ed) GaussView 03. Semichem Inc, Shawnee Mission, KS
35. Lee C, Yang WR, Parr G (1988) Phys Rev B 37:785–789
36. Becke AD (1993) J Chem Phys 98:5648–5652
37. Krishnan R, Binkley JS, Seeger R, Pople JA (1980) J Chem Phys 72:650–654
38. Singh DK, Srivastava SK, Schlücker S, Singh RK, Asthana BP (2011) J Raman Spectrosc 42:851–858
39. Singh S, Singh DK, Srivastva SK, Asthana BP (2011) Vibr Spectrosc 56:26–33
40. Singh DK, Srivastva SK, Asthana BP (2011) Chem Phys 380:24–33
41. Singh S, Singh DK, Srivastva SK, Asthana BP (2011) Z Phys Chem 225:723–740
42. Mennucci B, Tomasi J (1997) J Chem Phys 106:5151–5158
43. Mennucci B, Tomasi J, Cammi R, Cheeseman JR, Frisch MJ, Devlin FJ, Gabriel S, Stephens PJ (2002) J Phys Chem A 106:6102–6113
44. Buckingham AD, Fowler PW, Hutson JM (1988) Chem Rev 88:963–988
45. Asthana BP, Kiefer W (1982) Appl Spectrosc 36:250–257
46. Nygaard L, Nielsen JT, Kirchheiner J, Maltesen G, Rastrup-Andersen J, Soerensen GO (1969) J Mol Struct 3:491–500
47. Bernardi F, Bottoni A, Venturini A (1988) J Mol Struct (THEOCHEM) 163:173–189
48. Boys SF, Bernardi F (1970) Mol Phys 19:553–566
49. Simon S, Duran M, Dannemberg JJ (1996) J Chem Phys 105:11024–11031
50. Andersson MP, Uvdal P (2005) J Phys Chem A 109:2937–2941
51. Guirgis GA, Klaboe P, Shen S, Powell DL, Gruodis A, Aleksa V, Nielsen CJ, Tao J, Zheng C, Durig JR (2003) J Raman Spectrosc 34:322–336, and references cited therein
52. Polavarapu PL (1990) J Phys Chem 94:8106–8112
53. Bondarev AF, Mardaeva AI (1973) Opt Spectrosc 35:286–288
54. Fischer SF, Laubereau A (1978) Chem Phys Lett 55:189–196